Journal of Materials Chemistry A

Topotactic Phase Transformation of Lithiated Spinel to Layered LiMn0.5Ni0.5O2: The Interaction of 3-D and 2-D Li-ion Diffusion

Journal:	*Journal of Materials Chemistry A*
Manuscript ID	TA-ART-09-2024-006238.R1
Article Type:	Paper
Date Submitted by the Author:	22-Nov-2024
Complete List of Authors:	Shi, Boyu; Argonne National Laboratory, Chemical Sciences and Engineering Division Gim, Jihyeon; Argonne National Laboratory, Chemical Sciences and Engineering Division Li, Tianyi; Argonne National Laboratory, X-ray Science Division Koirala, Krishna Prasad; Pacific Northwest National Laboratory, Physical and Computational Sciences Directorate Wang, Chongmin; Pacific Northwest National Laboratory, Environmental Molecular Sciences Laboratory Hou, Dewen; Argonne National Laboratory, Center for Nanoscale Materials ; Boise State University, Micron School of Materials Science and Engineering Liu, Yuzi; Argonne National Laboratory, Center for Nanoscale Materials Jorne, Jacob; University of Rochester, Department of Chemical Engineering Croy, Jason; Argonne National Laboratory, Chemical Sciences and Engineering Division Thackeray, Michael; Argonne National Laboratory, Chemical Sciences and Engineering Division Lee, Eungje; Argonne National Laboratory, Chemical Sciences and Engineering Division

Topotactic Phase Transformation of Lithiated Spinel to Layered $LiMn_{0.5}Ni_{0.5}O_2$: The Interaction of 3-D and 2-D Li-ion Diffusion

Boyu Shi[1], Jihyeon Gim[1], Tianyi Li[2], Krishna Koirala[3], Chongmin Wang[4], Dewen Hou[5,6], Yuzi Liu[5], Jacob Jorne[7], Jason R. Croy[1], Michael M. Thackeray[1], and Eungje Lee[1,*]

[1] Electrochemical Energy Storage Department, Chemical Sciences and Engineering Division, Argonne National Laboratory, Lemont, IL 60439, USA

[2] X-ray Science Division, Advanced Photon Source, Argonne National Laboratory, Lemont, IL 60439, USA

[3] Physical and Computational Sciences Directorate, Pacific Northwest National Laboratory, Richland, WA 99354, USA

[4] Environmental Molecular Sciences Laboratory, Pacific Northwest National Laboratory, Richland, WA 99354, USA

[5] Nanoscience and Technology Division, Argonne National Laboratory, Lemont, IL 60439, USA

[6] Micron School of Materials Science and Engineering, Boise State University, Boise, Idaho 83725, USA

[7] Department of Chemical Engineering, University of Rochester, Rochester, NY 14627, USA

*Corresponding author: eungje.lee@anl.gov

Abstract

This study investigates the structural evolution of $LiMn_{0.5}Ni_{0.5}O_2$ cathode materials for Li-ion batteries as a function of synthesis temperature and its effect on electrochemical performance. It is demonstrated that, as the synthesis temperature increases from 400 to 900 °C, a gradual topotactic transformation occurs between a lithiated spinel structure, denoted herein as "lithium-excess spinel" LxS-$LiMn_{0.5}Ni_{0.5}O_2$ (or LxS-LMNO), and the well-known layered $LiMn_{0.5}Ni_{0.5}O_2$ structure prepared at high temperature, HT-$LiMn_{0.5}Ni_{0.5}O_2$ (HT-LMNO). The electrochemical capacity of the $LiMn_{0.5}Ni_{0.5}O_2$ electrodes follows a parabolic trend with increasing synthesis temperature, which is attributed primarily to the gradual transformation of 3-dimensional (3-D) to 2-dimensional (2-D) diffusion pathways for the Li ions. When synthesized at 400 °C, LxS-$LiMn_{0.5}Ni_{0.5}O_2$ electrodes perform well, benefitting from the 3-D network of channels within the LxS structure. By contrast, when prepared at 500-700 °C, $LiMn_{0.5}Ni_{0.5}O_2$ electrodes operate poorly, which is attributed to the formation of locally disordered structural arrangements that impede Li-ion diffusion. Such an increase in local disorder in the mid-temperature synthesis range is attributed to the structural frustration between the lithium-excess spinal and layered end-members. The transformation from the locally disordered to more ordered layered components between 700 °C and 900 °C enhances electrochemical performance. The study opens new avenues for designing next-generation Mn-rich cathode materials by fine-tuning the synthesis conditions as well as the composition and structure of LxS-LMNO electrodes.

1. Introduction

Non-aqueous lithium-ion batteries are used widely in applications such as portable electronics, electric vehicles (EVs), and the electrical grid, reflecting their pivotal role in advancing energy storage systems.[1, 2] The cathode material is a vitally important component of these batteries because it plays a major role in dictating each cell's energy density, power density, and cycling stability.[3] $LiCoO_2$ (LCO), the first "Li-ion" cathode material introduced commercially by Sony Corporation in 1991, marked a significant milestone because of its high energy density and structural robustness during long-term electrochemical cycling[4] relative to rechargeable aqueous systems such as nickel-cadmium and nickel-metal hydride batteries.[5] Nevertheless, LCO faces intrinsic challenges regarding the secure, cost-effective, and limited supply of cobalt, which have restricted its broader adoption in lithium-ion batteries besides portable electronic devices. These limitations have shifted international research toward nickel-rich cathode materials such as $LiNi_xCo_yAl_zO_2$ (NCA) and $LiNi_xMn_yCo_zO_2$ (NMC) in which cobalt is less than 33% of the transition-metal content. However, cathodes with a high Ni content face challenges such as capacity degradation and thermodynamic instability.[6] Additionally, although Ni is considered as an earth-abundant element and plays a critical role in high-performance vehicle applications, concerns over Ni demand and the stability of supply chains have already surfaced, and thus the cost-effectiveness of high-Ni cathodes could remain an issue. Consequently, there persists a substantial demand for the development of high energy density cathodes with excellent stability based on economically viable and abundantly available elements, such as manganese.[7]

In this context, the layered $LiMn_{0.5}Ni_{0.5}O_2$ cathode, first reported by Ohzuku et al. in 2001,[8] is being revisited as a Co-free and low-Ni baseline material for the further development of Mn-based cathodes. $LiMn_{0.5}Ni_{0.5}O_2$ offers an attractive theoretical capacity (283 mAh/g) and a lower-cost alternative with enhanced operational safety relative to cobalt- and nickel-rich materials. When synthesized at high temperature (HT), typically 800-900 °C, HT-$LiMn_{0.5}Ni_{0.5}O_2$ adopts a slightly disordered (10-11%), layered $LiCoO_2$-type structure (*R*-3*m* symmetry) with an architecture that offers predominantly 2-D interstitial spaces for Li-ion diffusion.[9] The redox reaction occurs primarily on the nickel ions, whereas the manganese ions remain largely inactive in a tetravalent state, thereby suppressing manganese dissolution and stabilizing the electrode structure.[10-12] Layered HT-$LiMn_{0.5}Ni_{0.5}O_2$ electrodes are also notable for their modest volume change during electrochemical charge and discharge.[13] Despite these advantages, HT-

$LiMn_{0.5}Ni_{0.5}O_2$, with its relatively high manganese content, has not yet been commercialized because of its inferior electrode capacity and rate performance relative to layered NMC compositions, particularly those with high nickel content.

Recently, our group reported a novel LT-$LiMn_{0.5}Ni_{0.5}O_2$ cathode material, where LT refers to its "low temperature" synthesis (400 °C).[14] In stark contrast to the layered high-temperature analog, HT-$LiMn_{0.5}Ni_{0.5}O_2$, X-ray diffraction (XRD) data and high-angle annular dark-field scanning transmission electron microscopy (HAADF-STEM) analyses have shown that LT-$LiMn_{0.5}Ni_{0.5}O_2$, alternatively LT-Li_2MnNiO_4, consists predominantly of a cubic lithiated spinel structure with an electrochemical profile that is distinct from previously-reported Co-containing lithiated spinel electrodes LT-$Li_2Co_{2-x}M_xO_4$ (M=Ni, Al, Mn, Ga).[15-19] Furthermore, unlike the cubic spinels $LiMn_2O_4$ (LMO)[20] and $LiMn_{1.5}Ni_{0.5}O_4$ (LMNO)[21] that transform anisotropically on lithiation to tetragonal $Li_2Mn_2O_4$ and $Li_2Mn_{1.5}Ni_{0.5}O_4$, respectively, the discharged lithiated spinel electrode LT-Li_2MnNiO_4 and its delithiated (charged) LT-$Li_{2-x}MnNiO_4$ ($0<x<2$) products maintain cubic symmetry during electrochemical cycling, thereby providing greater structural stability and reversibility. In this case, charge transfer in LT-$Li_{2-x}MnNiO_4$ electrodes occurs predominantly on the nickel and oxygen ions rather than the manganese ions.[22, 23] Detailed high-resolution transmission electron microscopy (HRTEM) images have revealed that LT-Li_2MnNiO_4 particles also contain a minor amount of disordered layered and rock salt-like domains interspersed within the cubic lithiated spinel (Li_2MnNiO_4) matrix. A conceptual and schematic illustration of an LT-Li_2MnNiO_4 structure prepared at 400 °C is shown in Figure 1; it highlights the structural compatibility of a lithiated spinel component with partially disordered layered and rock salt components and the interaction between 3-D and 2-D Li-ion diffusion pathways within a common cubic close-packed oxygen array. To reflect the unique phase combination, we designate this new class of materials as LxS-LMNO, where LxS represents the lithium (L) excess (xS) content within the spinel structure and the potential integration of partially disordered layered (L) domains into the cubic lithiated spinel (S) phase. The name captures the potential interplay between the cubic lithiated spinel, partially disordered layered, and disordered rock salt structural domains. While LxS serves as a comprehensive term for the entire system, we reserve "lithiated spinel" specifically for the cubic lithiated spinel phase domain within LxS. Additionally, the designation LxS distinguishes these materials from the well-known spinel composition $LiMn_{1.5}Ni_{0.5}O_4$ (LMNO)[21] and high-temperature layered HT-$LiMn_{0.5}Ni_{0.5}O_2$ (HT-LMNO) structures.

A significant advantage of LxS-LMNO (Li_2MnNiO_4) electrodes is that they offer almost twice the practical capacity of the stoichiometric Mn-rich spinels $LiMn_2O_4$ and $LiMn_{1.5}Ni_{0.5}O_4$ that operate reversibly at approximately 4.0 and 4.6 V vs. Li^0, respectively. These electrochemical reactions correspond to the extraction of one Li ion per formula unit with theoretical electrode capacities of 148.3 and 147.5 mAh/g, respectively; the cells lose capacity if cycled below 3 V. In contrast, LxS-LMNO electrodes provide an initial discharge capacity of 225 mAh/g, most of which is above 3 V, with 96% capacity retention after 50 cycles.[14] We note here that the LxS-LMNO at 5V delivers a specific energy of ~800 Wh/kg_{oxide}. And, while specific energy is not a stand-alone metric in evaluating practical performance, this energy is delivered without the use of cobalt and with a manganese content of 50%. This energy is on par, or better, than other cathodes of interest such as the lithium- and manganese-rich (LMR) and disordered rock salts (DRX) and reiterates the potential of LxS within the earth-abundant cathode space. Furthermore, it appears that the 3-D interstitial spaces of the $MnNiO_4$ spinel framework in delithiated LxS-LMNO ($Li_{2-x}MnNiO_4$) electrodes allow faster lithium diffusion kinetics relative to the 2-D spaces in disordered layered HT-$LiMn_{0.5}Ni_{0.5}O_2$. In addition to its potential as a stand-alone high-performance cathode, the robust 3-D framework of LxS-LMNO structures provides a unique opportunity to exploit it as a stabilizing component in high-capacity layered and Mn-rich cathode materials.[22, 23]

Here, we report on the gradual topotactic structural transformation of cubic lithiated spinel LxS-LMNO (Li_2MnNiO_4) to trigonal layered HT-$LiMn_{0.5}Ni_{0.5}O_2$ when heated from 400 to 900 °C in air and its impact on electrochemical performance as a function of the synthesis temperature. In addition, we analyze the unique structural transformation in the Li-Ni-Mn-O system, contrasting it with the two-phase transformation behavior observed in the Li-Co-(Ni)-O system. This research aims to elucidate the relationships among synthesis, structure, and electrochemical properties in LxS-LMNO materials, potentially guiding future developments of these new cathode materials.

2. Experimental Methods

Materials synthesis

A $Mn_{0.50}Ni_{0.50}(OH)_2$ precursor was prepared by co-precipitation of manganese sulfate ($MnSO_4$) and nickel sulfate ($NiSO_4$) in an aqueous solution using a continuous stirred-tank reactor (CSTR), as described in detail elsewhere.[24] Various $LiMn_{0.5}Ni_{0.5}O_2$ cathode structures were synthesized, first, by thoroughly mixing stoichiometric amounts of the $Mn_{0.50}Ni_{0.50}(OH)_2$ precursor

with lithium carbonate (Li_2CO_3, >99%) using a mortar and pestle and, thereafter, by calcining the mixtures in air from 400 to 900 °C with calcination times that varied from 72 h to 15 h, respectively. The heating rate was 2 °C/min, while cooling was uncontrolled. Because of the structural changes that occur over this temperature range, these samples are referenced hereafter in terms of their synthesis temperature, i.e., in incremental steps of 100 °C from LMNO400 to LMNO900 (Table 1).

Materials characterization

High-resolution synchrotron X-ray diffraction (HR-XRD) patterns of the LMNO400 to LMNO900 samples were collected in the transmission mode at beamline 11-ID-C of the Advanced Photon Source at Argonne National Laboratory. The calibrated X-ray wavelength was 0.1173 Å. The samples were sealed in a Kapton tube in an Ar-filled glovebox prior to data collection. Rietveld refinement analyses of the HR-XRD patterns were conducted using GSAS II software.

The morphologies of the LMNO400-900 electrode samples were investigated by scanning electron microscopy (SEM, JEOL JCM-6000Plus). Transmission electron microscopy (TEM) specimens of cathode particles were prepared by dispersing the particles onto lacey carbon grids within an Ar-filled glovebox. TEM imaging was performed at the Pacific Northwest National Laboratory in the high-angle annular dark-field (HAADF) mode using an aberration-corrected Spectra-Ultra scanning/transmission electron microscope (S/TEM) operated at 300 kV. For HAADF imaging, the convergence semi-angle was set to 30 mrad, and signals were collected over semi-angles ranging from 68 to 200 mrad at a probe current of 25 pA, effectively minimizing the major effects of the electron beam on the sample. High-resolution transmission electron microscopy (HR-TEM) images were also collected using a JEOL JEM2100F microscope (operating voltage of 200 kV) at the Center for Nanoscale Materials at Argonne National Laboratory.

Electrochemical evaluation

The electrochemical behavior of the LMNO400-900 cathodes was monitored in lithium coin cells (Hohsen, size 2032). A slurry was first prepared by thoroughly mixing 84 wt% LMNO powder, 8 wt% Super P carbon, and 8 wt% polyvinylidene difluoride (PVDF) binder in N-methyl-2-pyrrolidone (NMP). The slurries were then coated on an aluminum foil current collector

(thickness = 20 μm) using a stainless steel doctor blade. The laminated cathodes were dried at 70 °C in a heating chamber overnight before being cut into small discs approximately 14 mm in diameter. The mass loading of active material was ~4.4 mg/cm^2. The electrochemical cells were assembled in an Ar-filled glovebox (O_2 < 1 ppm, H_2O < 1 ppm) using a Celgard 2325 separator and a lithium metal disc as the anode. The electrolyte consisted of 1.2M lithium hexafluorophosphate ($LiPF_6$) in a 3:7 mixture of ethylene carbonate and ethyl methyl carbonate. Cells were cycled in a temperature-controlled chamber at 30 °C under a constant current density of 15 mA/g (0.15C; 1C = 100 mA/g) between 5.0 and 2.5 V vs. Li/Li$^+$ using a MACCOR battery testing system.

3. Results and Discussion

Structural analysis (XRD and HR-TEM): cubic (Fd-3m) vs. trigonal (R-3m) symmetry

High-resolution synchrotron XRD patterns of $LiMn_{0.5}Ni_{0.5}O_2$ samples, synthesized at temperatures ranging from 400 to 900 °C, are shown in Figure 2a. The XRD pattern of LMNO400 could be indexed to a cubic LxS-$LiMn_{0.5}Ni_{0.5}O_2$ structure (*Fd*-3*m* symmetry) with dominant lithiated spinel character interspersed with disordered layered and rock salt components, as observed by HAADF-STEM and depicted in the schematic illustration in Figure 1, which was consistent with our previous findings.[14] At the other extreme, the XRD patterns of LMNO800 and LMNO900 could be indexed to the well-known and partially disordered layered HT-$LiMn_{0.5}Ni_{0.5}O_2$ phase (*R*-3*m* symmetry), as evident from the splitting of the (222) and (440) peaks of the lithiated spinel structure into the (006)/(012) peaks and (018)/(110) peaks of the layered structure, respectively (Figures 2b and 2c). In contrast, a clear description of the structural arrangements in the LMNO500-700 samples that had been heated to intermediate temperatures proved to be difficult because of the broad, overlapping (222) and (440) peaks and the onset of the transformation of the lithiated spinel component toward a layered configuration over this temperature range. Later sections of this paper delve deeper into the complexity of the structural and electrochemical property relationships of $LiMn_{0.5}Ni_{0.5}O_2$ electrodes when prepared at these intermediate temperatures.

Of particular relevance to this work is the hypothetical situation, first reported by Rossen et al. in 1993:[25] If an ideal layered structure, such as $LiCoO_2$ (*R*-3*m* space group, *c/a* = 4.99), were to have an ideal cubic close-packed oxygen lattice (for which the corresponding *c/a* ratio would

be 4.90), then the nearest-neighbor vector space of every atom in the layered structure would be identical to that of an ideal cubic lithiated spinel $Li_2Co_2O_4$ structure (*Fd*-3*m* symmetry), thereby generating identical XRD patterns. (See Rossen et al.[25] and Figure S1 for a detailed description and representation of this structural anomaly.) In such a case, it would not be possible to determine the relative amounts of the lithiated spinel and layered components in the overall structure. Nevertheless, the *c/a* ratio would still serve as a useful metric for monitoring the transformation of lithiated spinel LMNO400 to partially disordered, layered configurations at higher synthesis temperatures.

Rietveld refinements of the LMNO400-900 structures were first conducted using a layered model with trigonal *R*-3*m* symmetry (Figures S2a-f) in which the occupancy, x, of the lithium and transition metal (M) cations in the $[Li_{1-x}M_x]_{(3a)}[Li_xM_{1-x}]_{(3b)}O_2$ ($M=Ni_{1/2}Mn_{1/2}$) structure was varied to monitor the changes in: 1) the *c/a* ratio as a function of the synthesis temperature and 2) the degree of disordering of the lithium and transition metal ions, as summarized in Table 2.

The refined *c*/*a* ratio (4.903) of the oxygen sublattice in LMNO400 is in excellent agreement with the value for a perfect cubic close-packed oxygen array (4.899). When heated between 500 and 600 °C, the sharp increase of the *c*/*a* ratio from 4.910 in LMNO500 to 4.934 in LMNO600 reflects a distinct crystallographic change, which is consistent with the onset of a transformation of the lithiated spinel component toward a disordered layered/rock salt configuration. For the high-temperature products LMNO800 and LMNO900, the *c/a* ratio is 4.944 and 4.945, respectively, which is consistent with prior reports for the strongly layered product HT-$LiMn_{0.5}Ni_{0.5}O_2$ (Figure 3a).[26, 27] Note that the *a* lattice parameter remains essentially constant during the heating process and that the *c*/*a* ratios of the HT-LMNO800 and HT-LMNO900 products are significantly lower than those for perfectly layered HT-$LiCoO_2$ and nickel-substituted HT-$LiCo_{1-x}Ni_xO_2$ (LCNO $0\leq x\leq 0.2$) structures in which *c/a* = 4.99 above 700 °C.[16]

The variation of cation disorder in the layered LMNO400-900 structures (*R*-3*m* symmetry) as a function of synthesis temperature is summarized in Table 2 and Figure 3b. The extent of Li:M exchange in the products, where M=Mn+Ni, provides a good approximation of the *average* disorder of the lithium and M cations in alternate layers of the close-packed oxygen array. When refined with trigonal *R*-3*m* symmetry, the LMNO400 product, which is composed predominantly of a lithiated spinel component and a smaller amount of disordered layered/rock salt character, revealed that the *average* disorder between the Li and M cations in alternate layers was 17.89%,

in reasonably good agreement with the values reported in our first disclosure of LMNO400 (16.67%).[14] In contrast, refinement of the X-ray diffraction data of the high-temperature materials LMNO800 and LMNO900 showed significantly less disorder in the layered structure, viz., 10.6% and 10.1%, respectively, in good agreement with previously reported data on HT-$LiMn_{0.5}Ni_{0.5}O_2$.[9]

Given the crystallographic anomaly that exists in the X-ray diffraction patterns of LMNO400 with lithiated spinel and layered $LiMn_{0.5}Ni_{0.5}O_2$ components with a common cubic close-packed oxygen array, a Rietveld refinement of LMNO400 was also undertaken using cubic *Fd*-3*m* symmetry, the results of which are provided in Table 2 and Figure S2(g). In this case, the occupancy of the lithium and transition metal (M) ions was varied on the 16c and 16d octahedral sites of the lithiated spinel $[Li_{2-x}M_x]_{(16c)}[Li_xM_{2-x}]_{(16d)}O_4$ structure. Here, the extent of cation disorder (i.e., Li/M exchange) on the 16c and 16d octahedral sites of the LMNO400 model was determined to be 18.83%, which is similar to the extent of disorder in the layered model. As discussed in our previous report,[14] LMNO400 is a structurally integrated composite material containing lithiated spinel as a major phase and disordered layered and rock salt as minor components in a common cubic close-packed oxygen array. We believe that the higher value of the average cation disorder in LMNO400 can be attributed mostly to the highly disordered nature of the layered and rock salt components rather than the lithiated spinel phase. This argument is also supported by the TEM and electrochemical data of these materials that follow in this paper.

Representative HAADF-STEM images of LMNO400, 600, and 900 samples were obtained to probe their structural complexity and the transformation from lithiated spinel to layered atomic configurations as a function of their synthesis temperature. The images shown in Figures 4a-c corroborate the XRD data provided in the previous section: 1) The LMNO400 sample was dominated by lithiated spinel domains, structurally integrated with minor amounts of disordered layered (rock salt) domains (Figure 4a); 2) raising the synthesis temperature to 600 °C results in the absence of local, perfectly ordered, lithiated spinel domains and the formation of heavily disordered layered (rock salt) domains, as shown in Figures 4b, which is consistent with the trends of the *c/a* ratio and disordering ratio derived from the XRD data in Table 2; and 3) at 900 °C, a slightly disordered (10%) layered structure forms, as expected (Figure 4c). The HR-TEM images with a larger scale bar and Fast Fourier Transform (FFT) analyses demonstrate a similar transformation behavior (Figure S3). The TEM images illustrate the gradual topotactic phase transformation from lithiated spinel (LMNO400) to partially disordered (~10%) layered

(LMNO900) with "mid-temperature" samples, e.g., LMNO500-600, that are substantially disordered.

Electrochemistry

Li/LMNO400-900 cells were cycled between 2.5 and 5.0 V at a constant current (15 mA/g) to monitor the electrochemical behavior of the LMNO400-900 cathodes as a function of their synthesis temperature. Note that SEM images of the LMNO400-900 particles (Figure S4) show remarkably similar secondary particle morphology and size ranging from 5 to 20 μm, confirming that the electrochemical properties of the LMNO400-900 materials can be attributed to their unique atomic structures rather than particle morphological effects. Typical voltage profiles of these cells, as recorded on the second charge/discharge cycle, are provided in Figure 5a, while profiles normalized to remove the variations in electrode capacity are shown in Figure 5b, thereby allowing a clearer comparison of the electrochemical processes occurring at the cathode. Corresponding differential capacity (dQ/dV) plots of the Li/LMNO400 and Li/LMNO500 cells are shown in Figure 5c (top) while those of the Li/LMNO600-900 cells are provided in Figure 5c (bottom). The voltage profiles for the first charge/discharge cycle and the corresponding dQ/dV plots are shown in Figure S5. Table S1 provides the initial Coulombic efficiency. These electrochemical analyses complement the XRD and HR-TEM data described earlier in this paper. Despite the highly complex cathode structures, it is possible to make some tentative general assignments to the redox processes that occur during the early stages of electrochemical cycling. For example, the voltage profile and dQ/dV plot of the Li/LMNO400 cell show five distinct oxidation reactions during charge. The first two processes at approximately 3.6 and 3.7 V can be attributed to lithium extraction from the octahedral sites of the cubic lithiated spinel and neighboring disordered spinel/layered/rock-like configurations identified in the HAADF-STEM images (Figures 4a), during which the nickel ions are oxidized from a divalent to a trivalent state. The third oxidation process that occurs at ~4.4 V is irreversible and not yet understood, while the remaining two oxidation processes that occur at ~4.6 and ~4.7 V in Figure 5c are reversible and tentatively attributed to the extraction of lithium from the tetrahedral sites of the spinel-like configurations mentioned earlier. We suspect that the two high-voltage processes occur with further oxidation of the nickel ions and possibly some participation of the oxygen ions. The complex role of oxygen in these materials is beyond the scope of the work herein but is currently under investigation using

resonant inelastic x-ray spectroscopy (RIXS), a study to be published in due course. Note that the reversible extraction and reinsertion of lithium from the octahedral and tetrahedral sites of the lithiated spinel structure in the LMNO400 electrode are separated from each other by approximately 1 V. These processes are also coincident with the electrochemical behavior of the lithiated spinel $Li_2Mn_2O_4$ when lithium extraction from the octahedral and tetrahedral sites occurs at ~3V and ~4V, respectively, with the concomitant oxidation of the manganese ions.[28] Figure 5d shows the cycling data for all samples. These initial studies are performed, as is typical, in cells utilizing Li-metal anodes (i.e. large source of excess Li) where it can be concluded that loss of Li sites due to structural changes in the cathode is not significant, even when cycled between 4.7-2.5V. The best performer of these cathodes (LMNO400) was then cycled between 5.0-2.5 V to stress the material. Again, good performance is shown over 50 cycles.

When the synthesis temperature is raised to 500 °C, it is immediately clear from the electrochemical profiles of the second cycle in Figures 5a-c that the spinel component in the LMNO500 electrode is markedly suppressed while showing the remnants of a spinel-like profile at ~3.5 V and ~4.5 V during both charge and discharge. Furthermore, the dQ/dV plots in Figure 5c clearly show that increasing the synthesis temperature to 600-900 °C eliminates the formation of a lithiated spinel component in the LMNO electrode structure, as does the absence of spinel-related voltage plateaus at approximately ~3.5 and ~4.5 V. These high-temperature LMNO600-900 electrodes, therefore, adopt a gradually sloping voltage profile characteristic of a layered-type structure, the average voltage of which gradually increases as the synthesis temperature is raised from approximately 3.7 V for LMNO600 to 3.8 V for LMNO900. This electrochemical behavior is consistent with a reaction process that primarily involves the extraction and reinsertion of lithium predominantly from octahedral sites in a disordered layered/rock salt structure rather than the tetrahedral and octahedral sites in a spinel-type electrode structure.

The specific capacity of LMNO400-900 electrodes on the second discharge exhibits a parabolic relationship with synthesis temperature (Figure 6a). The rate performance for LMNO follows a similar trend, as illustrated in Figure S6a, which shows the relative capacity retained at a faster charge-discharge rate at 200 mA/g. (Complete capacity and voltage profile data at current densities from 15 – 300 mA/g are provided in Figures S6b and S7.) This parabolic behavior is interesting because the electrochemical performance of cathode materials generally decreases monotonically with decreasing synthesis temperature as a result of less ordered structures.[29] The

LMNO materials follow this expected trend when synthesized in the high-to-mid-temperature range, achieving capacities of 191 mAh/g and 171 mAh/g at 900°C and 700°C, respectively. However, as the calcination temperature drops below 700 °C, capacities increase to 225 mAh/g at 400°C. This distinct parabolic evolution in electrochemical performance can be attributed to a continuous topotactic phase transformation from a high-temperature layered phase (LMNO900) with 2-D Li-ion diffusion channels to a low-temperature, stabilized lithiated spinel phase (LMNO400) with 3-D Li-ion diffusion channels. Intermediate temperatures lead to highly disordered atomic configurations that interrupt either the layered 2-D or the spinel 3-D Li-ion conduction pathways in the electrode structure, at least locally, thereby lowering the electrode capacity as shown in Figure 6a and Figure S9. It should be noted that this frustrated structure may still preserve overall lithium diffusion channels (in spite of the possibility of forming several isolated domains), distinguishing it from a completely disordered rock salt phase where lithium diffusion is entirely blocked. This distinction can be demonstrated by the nearly identical electrochemical performance of LMNO400-900 electrodes when cycled at 50 °C (Figure 6b). The 20-degree increase in the operating temperature of the cells largely overcame the diffusional barriers for lithium transport in the LMNO500-700 electrodes, with all three cells yielding capacities of approximately 220 mAh/g. In addition, the 1st and 2nd cycle charge and discharge curves for LMNO400-900 samples are shown in Figure S8.

Finally, it is worthwhile to compare the electrochemical and structural behavior of LMNO400 electrodes with the results of our earlier study of Mn-free $LiCo_{0.1}Ni_{0.9}O_2$ (LCNO400) lithiated spinel electrodes.[16] Whereas LMNO400 electrodes are composed predominantly of lithiated spinel domains intergrown with disordered layered domains, LCNO400 electrodes can be synthesized as a single-phase lithiated spinel product from which approximately one-half of the lithium ions (~45%, ~125 mAh/g) can be extracted electrochemically in cells when charged to 4.2 V without structural damage to the spinel framework. Note, however, that when LMNO400 electrodes are charged to 4.2 V, they are also more stable to electrochemical cycling, yielding approximately 115 mAh/g. However, when synthesized at 600 °C, LCNO600 electrodes exist as a composite structure of distinct and highly ordered lithiated spinel and layered domains, the latter developing progressively from the particle surface without hindering lithium diffusion,[16] in contrast to the severe disorder that occurs in the LMNO600 product during the conversion from a lithiated spinel to a layered configuration. For example, a STEM image of a LCNO600 particle in

Figure 7b reveals well-ordered, lithiated spinel and layered components that are clearly distinguishable with pronounced domain boundaries. In contrast, the LMNO600 particle in Figure 7a displays diffused domain boundaries, indicating a higher level of structural frustration and disorder. This comparative study between LMNO and LCNO electrodes is ongoing, the full results of which will be presented in due course.

4. Conclusions

The discovery of the cubic (*Fd*-3*m*) lithiated spinel $LiMn_{0.5}Ni_{0.5}O_2$ structure first reported in 2021[14] represents a significant advancement in the design of high-capacity cathode materials for Li-ion batteries based on earth-abundant manganese. When synthesized at 400 °C, the product, code-named LxS-LMNO400 to separate it from the many families of lithium-manganese-nickel-oxide compounds, also contains a minor disordered layered/rock salt component, both of which share a common cubic close-packed oxygen array (*c/a* ratio = 4.90). Increasing the synthesis temperature from 400 to 900 °C results in a steady transformation to the well-known, slightly disordered, layered $LiMn_{0.5}Ni_{0.5}O_2$ structure with a concomitant increase of the *c/a* ratio from 4.90 to 4.945. This is a unique transformation because it occurs with little change to the X-ray diffraction patterns, thereby closely mimicking the structural anomaly that would exist between an ideal lithiated spinel structure and an ideal layered structure if the oxygen array of both structures was perfectly cubic close-packed. Consequently, a novel parabolic dependence between electrochemical performance and synthesis temperature is observed. This dependence is attributed primarily to the gradual transformation of 3-D to 2-D diffusion pathways for the Li ions where LxS-$LiMn_{0.5}Ni_{0.5}O_2$ synthesized at 400 °C benefits from the 3-D network of channels within the LxS structure. In contrast, the gradual performance decrease for LMNO500-700 samples is attributed to the progressive transformation from lithiated spinel to a structurally frustrated phase in which significant cation disorder obstructs facile Li-ion diffusion pathways. The transformation from disorder to a less disordered layered structure between 700 and 900 °C temperatures leads to progressively improved electrochemical performance for LMNO800 and LMNO900 samples. These results provide valuable insights for the design of novel stabilized composite electrode materials and structures with interconnected 2-D and 3-D diffusion pathways for the lithium ions.

Author Contributions

Boyu Shi: conceptualization, investigation, data curation, visualization, writing – original draft. Jihyeon Gim: investigation, validation. Tianyi Li: investigation, data curation. Krishna Koirala: investigation, data curation. Chongmin Wang: validation. Dewen Hou: investigation, data curation. Yuzi Liu: validation. Jacob Jorne: validation. Jason R. Croy: funding acquisition, writing – review & editing. Michael M. Thackeray: conceptualization, writing – review & editing. Eungje Lee: conceptualization, project administration, supervision, writing – review & editing.

Conflict of interest

There are no conflicts of interest to declare.

Acknowledgements

Support from the Office of Vehicle Technologies of the U.S. Department of Energy (DOE), particularly from Tien Duong, is gratefully acknowledged. This research project used 11-ID-C resources of the Advanced Photon Source, a U.S. DOE Office of Science User Facility operated for the DOE Office of Science by Argonne National Laboratory under Contract No. DE-AC02-06CH11357. Work performed at the Center for Nanoscale Materials, a U.S. DOE Office of Science User Facility, was supported by the U.S. DOE Office of Basic Energy Sciences under Contract No. DE-AC02-06CH11357.

Part of the electron microscopy work was carried out by using a microscope funded by a grant from the Washington State Department of Commerce's Clean Energy Fund and was conducted at the William R. Wiley Environmental Molecular Sciences Laboratory (EMSL), a national scientific User Facility sponsored by U.S. DOE's Office of Biological and Environmental Research and located at PNNL. PNNL is operated by Battelle for the U.S. DOE under Contract DE-AC05-76RL01830.

References

1. M. S. Whittingham, *Chem. Rev.*, 2004, **104**, 4271-4301.
2. N. Nitta, F. Wu, J. T. Lee and G. Yushkin, *Mater. Today*, 2015, **18**, 252-264.
3. A. Manthiram, *Nat. Commun.*, 2020, **11**, 1550.
4. K. Ozawa, *Solid State Ionics*, 1994, **69**, 212-221.
5. L. Wang, J. Wang, L. Wang, M. Zhang, R. Wang, and C. Zhan, *Int. J. Miner. Metall. Mater.*, 2022, **29**, 925-941.
6. J. Kim, H. Lee, H. Cha, M. Yoon, M. Park, and J. Cho, *Advan. Energy Mater.*, 2018, **8**, 1702028.
7. M. M. Thackeray, J. R. Croy, E. Lee, A. Gutierrez, M. He, J. S. Park, B. T. Yonemoto, B. R. Long, J. D. Blauwkamp, C. S. Johnson, Y. Shin and W. I. F. David, *Sustainable Energy Fuels*, 2018, **2**, 1375-1397
8. T. Ohzuku and Y. Makimura, *Chem. Lett.*, 2001, **30**, 744-745.
9. Y. S. Meng, G. Ceder, C. P. Grey, W. S. Yoon, M. Jiang, J. Bréger, and Y. Shao-Horn, *Chem. Mater.*, 2005, **17**, 2386-2394.
10. X. Meng, S. Dou, and W.-l. Wang, *J. Power Sources*, 2008, **184**, 489-493.
11. Z. Liu, H. Zheng, L. Tan, S. Yuan, and H. Yin, *Energy Technol.*, 2018, **6**, 1302-1309.
12. A. Kropf, C. Johnson, J. Vaughey, and M. Thackeray, *Phys. Scr.*, 2005, **2005**, 274.
13. X.-Q. Yang, J. McBreen, W.-S. Yoon, and C. P. Grey, *Electrochem. Commun.*, 2002, **4**, 649-654.
14. B. Shi, J. Gim, L. Li, C. Wang, A. Vu, J. R. Croy, M. M. Thackeray, and E. Lee, *Chem. Commun.*, 2021, **57**, 11009-11012.
15. R. Gummow, M. Thackeray, W. David, and S. Hull, *Mater. Res. Bull.*, 1992, **27**, 327-337.
16. E. Lee, J. Blauwkamp, F. C. Castro, J. Wu, V. P. Dravid, P. Yan, C. Wang, S. Kim, C. Wolverton, and R. Benedek, *ACS Appl. Mater. Interfaces*, 2016, **8**, 27720-27729.
17. E. Lee, B. J. Kwon, F. Dogan, Y. Ren, J. R. Croy, and M. M. Thackeray, *ACS Appl. Energy Mater.*, 2019, **2**, 6170-6175.
18. K. Ku, J. Han, L. Li, J. Gim, J. Park, B. Shi, Y. Liang, A. Stark, C. Wang, J. R. Croy, M. M. Thackeray, J. Libera, and E. Lee, *J. Electrochem. Soc.*, 2023, **170**, 050511.

19. E. Gonzalo, E. Morán, C. Parada, and H. Ehrenberg, *Mater. Chem. Phys.*, 2010, **121**, 484-488.
20. M. M. Thackeray, W. I. David, P. G. Bruce, and J. B. Goodenough, *Mater. Res. Bull.*, 1983, **18**, 461-472.
21. D. Liu, W. Zhu, J. Trottier, C. Gagnon, F. Barray, A. Guerfi, A. Mauger, H. Groult, C. Julien, and J. Goodenough, *RSC Adv.*, 2014, **4**, 154-167.
22. M. M. Thackeray, *Advan. Energy Mater.*, 2020, **11**, 2001117.
23. M. M. Thackeray, E. Lee, B. Shi, and J. R. Croy, *J. Electrochem. Soc.*, 2022, **169**, 020535.
24. Z. Feng, P. Barai, J. Gim, K. Yuan, Y. A. Wu, Y. Xie, Y. Liu, and V. Srinivasan, *J. Electrochem. Soc.*, 2018, **165**, A3077.
25. E. Rossen, J. N. Reimers, and J. R. Dahn, *Solid State Ionics*, 1993, **62**, 53-60.
26. S.-H. Kang, S.-H. Park, C. S. Johnson, and K. Amine, *J. Electrochem. Soc.*, 2007, **154**, A268.
27. W. Shin, J. C. Garcia, A. Vu, X. Ji, H. Iddir, and F. Dogan, *J. Phys. Chem. C*, 2022, **126**, 4276-4285.
28. J. B. Goodenough and K.-S. Park, *J. Am. Chem. Soc.*, 2013, **135**, 1167-1176.
29. X. Wang and H.-L. Zhang, *Inter. J. Electrochem. Sci.*, 2021, **16**, 151011.

Table 1. Sample code and synthesis conditions of LMNO400-900 materials.

Sample code	Synthesis temperature (°C)	Calcination time (h)
LMNO400	400	72
LMNO500	500	72
LMNO600	600	72
LMNO700	700	48
LMNO800	800	24
LMNO900	900	15

Table 2. Summary of Rietveld XRD refinements of the LMNO400-900 samples.

Sample	Space group	*a* (Å)	*c* (Å)	*c*/*a*	V (Å^3)	Li/M (M=Mn+Ni) exchange on octahedral sites (%)[†]	R_{wp}
LMNO400	*R*-3*m*	2.901	14.224	4.903	103.678	17.80	13.78
LMNO500		2.898	14.231	4.910	103.583	16.00	12.04
LMNO600		2.894	14.282	4.934	103.673	13.60	11.11
LMNO700		2.893	14.288	4.939	103.583	12.30	10.30
LMNO800		2.892	14.298	4.944	103.581	10.70	8.56
LMNO900		2.889	14.291	4.945	103.349	10.10	8.42
LMNO400	*Fd*-3*m*	8.208	-	-	553.15	18.83	11.81

[†]Exchange (% disorder) of Li and M ions on the octahedral 3a/3b sites (*R*-3*m*) and 16c/16d sites (*Fd*-3*m*).

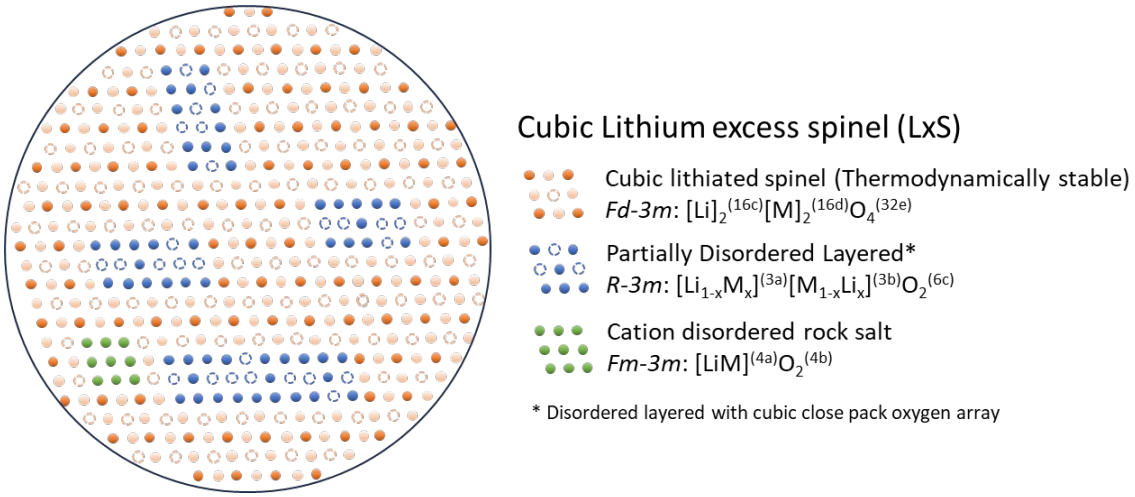

Figure 1. Schematic illustration of the LxS-LMNO structure with a cubic lithiated spinel phase structurally integrated with minor partially disordered layered and cation disordered rock salt domains.

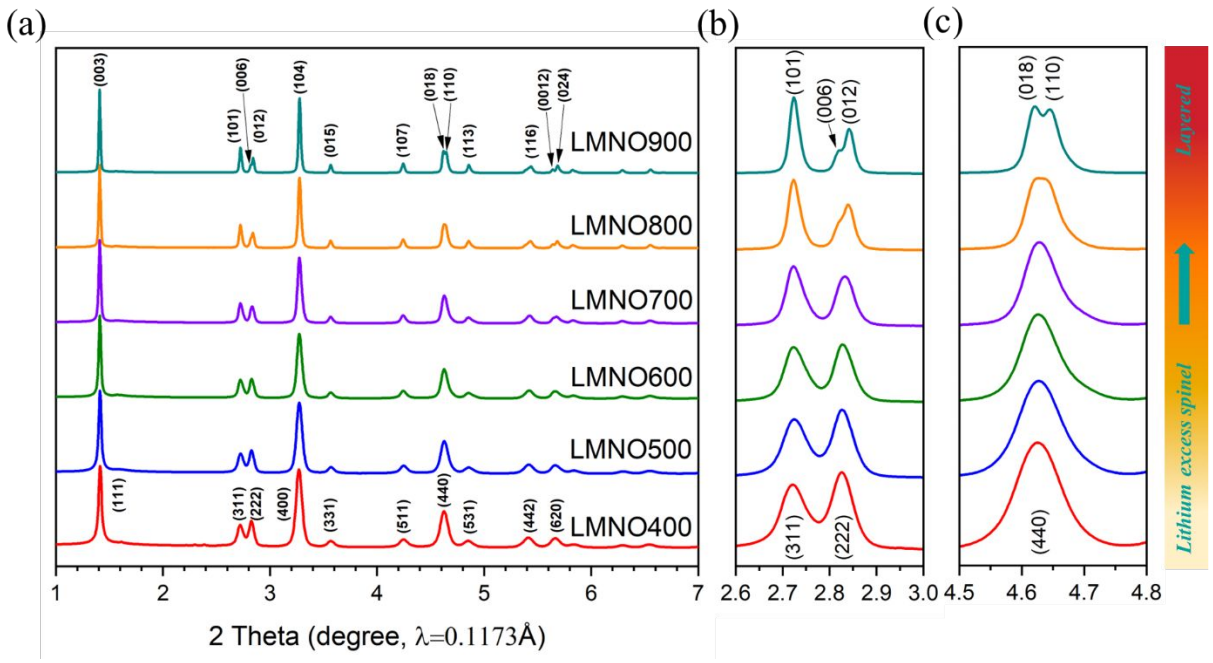

Figure 2. (a) Synchrotron XRD patterns of LMNO400-900 samples; (b, c) enlarged view of selected diffraction peaks, highlighting the extent of peak splitting as a function of the synthesis temperature.

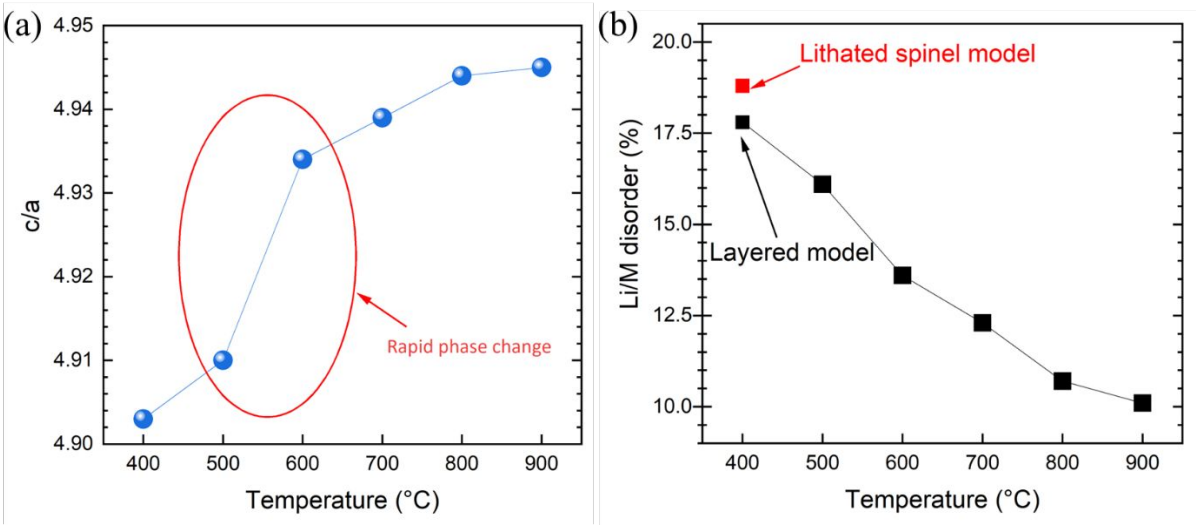

Figure 3. (a) Variation of the *c*/*a* ratio as a function of temperature, and (b) Li/M exchange ratios of LMNO400-900 samples as a function of synthesis temperature.

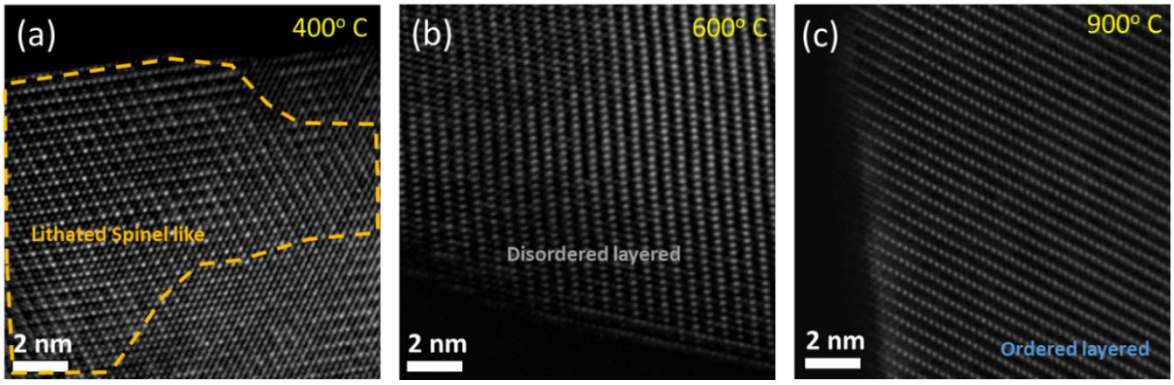

Figure 4. HAADF-STEM images of (a) LMNO400, (b) LMNO600, and (c) LMNO900.

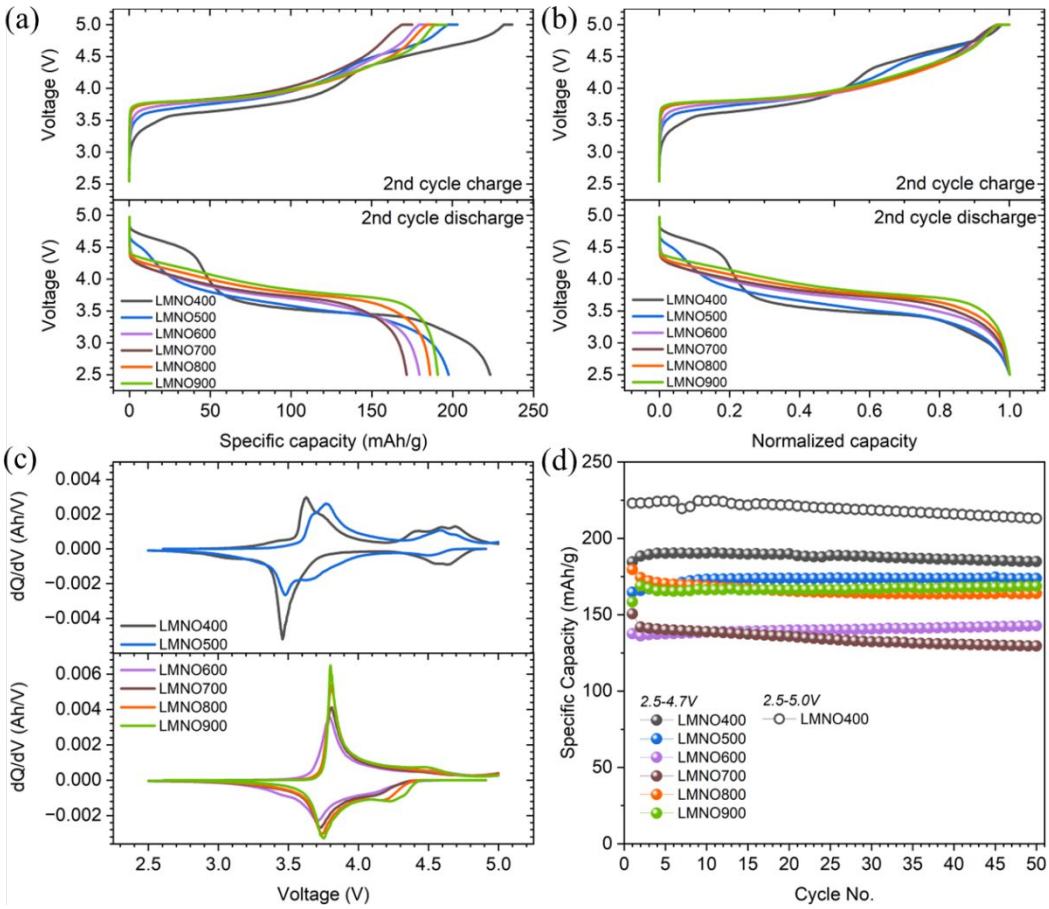

Figure 5. (a) 2nd charge-discharge voltage profiles, (b) normalized charge-discharge voltage profiles, (c) dQ/dV plots, and (d) capacity retention of Li/LMNO400-900 cells (i = 15 mA/g, 30 °C).

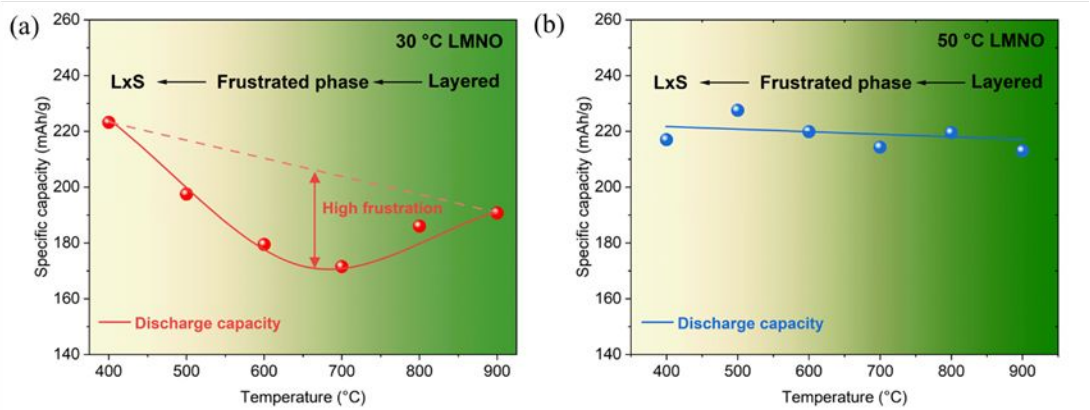

Figure 6. Specific capacity of the LMNO electrodes as a function of synthesis temperature, tested at (a) 30 °C and (b) 50 °C (2nd discharge capacity; V = 2.5-5.0 V vs. Li; *i* = 15 mA/g).

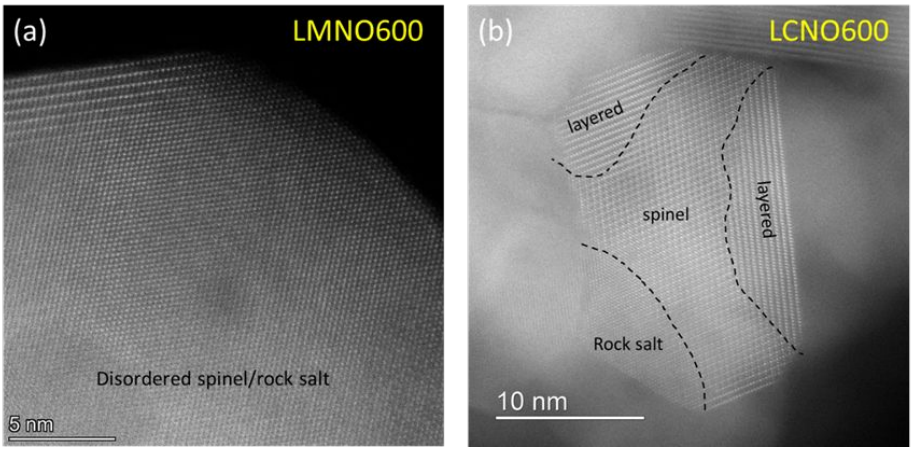

Figure 7. HAADF-STEM images showing (a) frustrated spinel/layered/rock salt domains for LMNO600 and (b) multi-phase composite of clearly distinguishable spinel/layered/rock salt phases domains for LCNO600. (Figure 7b is adapted with permission from E. Lee, J. Blauwkamp, F. C. Castro, J. Wu, V. P. Dravid, P. Yan, C. Wang, S. Kim, C. Wolverton, and R. Benedek, *ACS Applied Materials & Interfaces*, 2016, **8**, 27720-27729. Copyright 2016 American Chemical Society.[16])

Data Availability Statement

The data supporting this article have been included as part of the ESI.